Charge fluctuations in nano-scale capacitors

David T. Limmer, Céline Merlet, Mathieu Salanne, David Chandler, Paul A Madden, René van Roij, Benjamin Rotenberg

Charge fluctuations in nano-scale capacitors

David T. Limmer[1], Céline Merlet[2,3], Mathieu Salanne[2,3], David Chandler[1], Paul A. Madden[4], René van Roij[5], and Benjamin Rotenberg[2,3]
[1] *Department of Chemistry, University of California, Berkeley, CA-94720, USA*
[2] *UPMC Univ-Paris06 and CNRS, UMR 7195, PECSA, F-75005, Paris, France*
[3] *Réseau sur le Stockage Electrochimique de l'Energie (RS2E), FR CNRS 3459, France*
[4] *Department of Materials, University of Oxford, Parks Road, Oxford OX1 3PH, UK and*
[5] *Institute for Theoretical Physics, Utrecht University, 3584 CE Utrecht, The Netherlands*
(Dated: June 28, 2013)

The fluctuations of the charge on an electrode contain information on the microscopic correlations within the adjacent fluid and their effect on the electronic properties of the interface. We investigate these fluctuations using molecular dynamics simulations in a constant-potential ensemble with histogram reweighting techniques. This approach offers an efficient and accurate route to the differential capacitance and is broadly applicable. We demonstrate these methods with three different capacitors: pure water between platinum electrodes, and a pure as well as a solvent-based organic electrolyte each between graphite electrodes. The total charge distributions with the pure solvent and solvent-based electrolytes are remarkably Gaussian, while in the pure ionic liquid the total charge distribution displays distinct non-Gaussian features, suggesting significant potential-driven changes in the organization of the interfacial fluid.

PACS numbers: 68.08.-p,05.40.-a,82.47.Uv

The charge of an electrode in contact with a liquid and maintained at a constant potential undergoes thermal fluctuations that encode information on microscopic interfacial processes. Most common applications involving such interfaces, such as charge storage in dielectric or electrochemical double layer capacitors [1], electrochemistry, water purification, or the growing field of "blue energy" [2–4] utilize only the ability of the metal to aquire an average charge upon application of voltage. However, it is also possible to extract microscopic information on the interfacial processes from the fluctuation of the electrode charge. Our purpose here is to demonstrate this fact and to add to the tools available to exploit it.

As nanoscale devices become widely available, it is essential to better understand these fluctuations. Experimentally, this possibility is only rarely exploited, with the notable exceptions of electrochemical noise analysis to infer redox reaction rates and information on corrosion processes [5, 6] or more recently electrochemical correlation spectroscopy for single molecule detection and ultralow flow rate measurements in nanofluidic channels [7, 8]. The opportunities offered by such approaches remain however limited by the theoretical tools to interpret the signal and uncover the underlying processes.

Traditional mean-field treatments [9–13] including some models of electric current fluctuations [14, 15], ignore the fluctuations we consider. During the past decade, however, molecular simulations have been successfully applied to the study of various metallic electrodes (aluminum, platinum, graphite, nanoporous carbon) and electrolytes (aqueous and organic solutions, molten salts, ionic liquids) [5, 6, 13, 17–19]. In such simulations, it is essential to account for the polarization of the electrode by the ions. In turn, this polarization screens the (effective) interactions between the ions and thereby directly affects the structure and dynamics of the interface [22]. Analytical models accounting for the image charge induced on the electrode [23] remain limited to regular geometries. Nevertheless, efficient algorithms have been introduced to simulate electrodes in which the potential is maintained at a constant value [4, 13, 25]. The charge on each electrode atom then fluctuates in response to the thermal motion of the fluid and these fluctuations at any instant are significantly heterogeneous. See Figure 1.

Let $\mathcal{H} = K(\mathbf{p}^N) + U(\mathbf{r}^N, \mathbf{q})$ be the microscopic Hamiltonian of the system with ion positions $\mathbf{r}^N = \{\mathbf{r}_I\}_{I=1\ldots N}$, ion momenta $\mathbf{p}^N = \{\mathbf{p}_I\}_{I=1\ldots N}$ and electrode charge distribution $\mathbf{q} = \{q_i\}_{i=1\ldots 2M}$ with $2M$ including the atoms of both electrodes. The electrode atoms are fixed in space. The kinetic part K depends only on the ion momenta and its contribution to partition functions can be trivially integrated out. Thus in the following we focus only on the potential part U. The constant-potential ensemble is defined in terms of the potential of each electrode atom $\mathbf{\Psi}^0 = \{\Psi_i^0\}_{i=1\ldots 2M}$. In this ensemble, the charge distribution $\mathbf{q}$ in the electrodes fluctuates as a result of charge exchange with a reservoir, namely the external circuit which connects the two electrodes. Charging the capacitor from $\mathbf{q} = 0$ to a charge distribution $\mathbf{q}$ under fixed $\mathbf{\Psi}^0$ corresponds to a work exchange $\mathbf{q} \cdot \mathbf{\Psi}^0$ with this reservoir. Thus the probability of a state with ion positions $\mathbf{r}^N$ is

$$P(\mathbf{r}^N|\mathbf{\Psi}^0) = \frac{\int \mathrm{d}\mathbf{q}\ e^{-\beta U(\mathbf{r}^N,\mathbf{q})+\beta \mathbf{q}\cdot\mathbf{\Psi}^0}}{\int \mathrm{d}\mathbf{r}^N\ \mathrm{d}\mathbf{q}\ e^{-\beta U(\mathbf{r}^N,\mathbf{q})+\beta \mathbf{q}\cdot\mathbf{\Psi}^0}}\ , \qquad (1)$$

where $\beta = 1/k_\mathrm{B}T$, with k_B Boltzmann's constant and T the temperature.

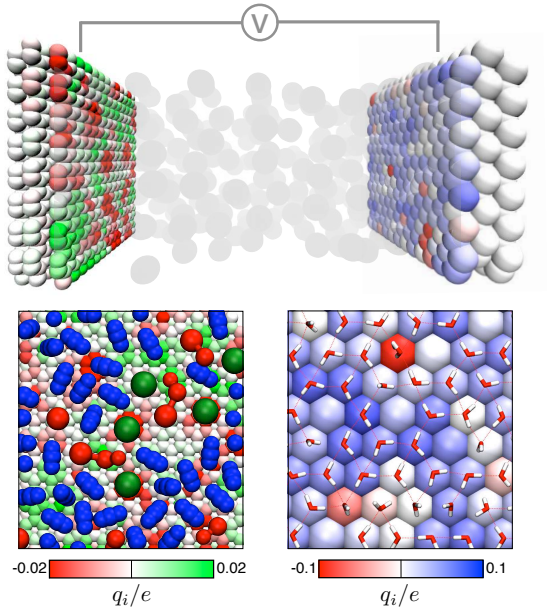

FIG. 1: Each capacitor consists of an electrolyte between two electrodes maintained at a constant potential difference. The color code on the electrode atoms indicates the instantaneous charge, q_i, with the corresponding scale shown at the bottom. The left panels show a graphite electrode and at the bottom left is a representative configuration of the first adlayer of the 1.5 M 1-butyl-3-methylimidazolium (red) hexafluorophosphate (green) in acetonitrile (blue) solution in contact with it. The right panels show the 111 crystal facet of a platinum electrode and at the bottom right is a representative configuration of the first adlayer of the water in contact with it.

The integrals can be computed using a saddle point expansion around the charge distribution $\mathbf{q}^*$ minimizing the term in the exponential, which satisfies:

$$\left.\frac{\partial U(\mathbf{r}^N,\mathbf{q})}{\partial \mathbf{q}}\right|_{\mathbf{q}=\mathbf{q}^*} = \mathbf{\Psi}^0 \ , \tag{2}$$

i.e. such that the potential on each atom is the imposed one. As shown in Supplementary Informations [26], the probability of a state with ion positions $\mathbf{r}^N$ (and corresponding charge distribution $\mathbf{q}^*$) can be expressed exactly using the Legendre transform $\mathcal{U}(\mathbf{r}^N,\mathbf{\Psi}^0) = U(\mathbf{r}^N,\mathbf{q}^*) - \mathbf{q}^*\cdot\mathbf{\Psi}^0$ as $P(\mathbf{r}^N|\mathbf{\Psi}^0) = e^{-\beta\mathcal{U}(\mathbf{r}^N,\mathbf{\Psi}^0)}/\mathcal{Z}(\mathbf{\Psi}^0)$, with $\mathcal{Z}(\mathbf{\Psi}^0) = \int \mathrm{d}\mathbf{r}^N\ e^{-\beta\mathcal{U}(\mathbf{r}^N,\mathbf{\Psi}^0)}$.

In practice one is only interested in the case where the potential can take only two values, namely $\Psi_i^0 = \Psi_+^0$ for all atoms in the positive electrode and $\Psi_i^0 = \Psi_-^0$ for all atoms in the negative electrode. This corresponds to the condition of a constant potential inside a metal (perfect conductor). In that case the additional energy term simplifies to $\mathbf{q}^*\cdot\mathbf{\Psi}^0 = \sum_{i\in\pm} q_i^*\Psi_i^0 = Q\Delta\Psi$, with $Q = Q^+ = -Q^-$ the total charge of the positive electrode and $\Delta\Psi = \Psi_+^0 - \Psi_-^0$ the potential difference between the electrodes. Note that the sign convention to label the electrodes does not matter. Moreover, the probability of a state, hence any observable property, depends only on $\Delta\Psi$ and not on the absolute value of the potentials, which are defined with respect to a reference electrode not present in the system and which provides charge to the electrodes. Using the above result, we finally rewrite the probability as

$$P(\mathbf{r}^N|\Delta\Psi) = \frac{e^{-\beta U(\mathbf{r}^N,\mathbf{q}^*)+\beta Q\Delta\Psi}}{\mathcal{Z}(\Delta\Psi)} \ , \tag{3}$$

with the partition function

$$\mathcal{Z}(\Delta\Psi) = e^{-\beta\mathcal{F}(\Delta\Psi)} = \int \mathrm{d}\mathbf{r}^N\ e^{-\beta U(\mathbf{r}^N,\mathbf{q}^*)+\beta Q\Delta\Psi} \ , \tag{4}$$

and $\mathcal{F}$ the associated free energy. In this ensemble, the average value of any observable $A(\mathbf{r}^N,\mathbf{q}^*)$ is computed as

$$\langle A\rangle = \int \mathrm{d}\mathbf{r}^N\ P(\mathbf{r}^N|\Delta\Psi)A(\mathbf{r}^N,\mathbf{q}^*) \ , \tag{5}$$

where one should keep in mind that the charge distribution $\mathbf{q}^*$ is not a free variable, as it is determined for each ion configuration $\mathbf{r}^N$ by Eq. 2. The average total charge determines the integral capacitance $\mathrm{C_{int}} = \langle Q\rangle/\Delta\Psi$, whereas the differential capacitance is related to the variance of the total charge distribution:

$$\mathrm{C_{diff}} = \frac{\partial\langle Q\rangle}{\partial\Delta\Psi} = \beta\left\langle\delta Q^2\right\rangle \ , \tag{6}$$

with $\delta Q = Q - \langle Q\rangle$. This fluctuation-dissipation relation, which can be derived by considering the derivatives of $\mathcal{Z}$ with respect to $\Delta\Psi$ [26], is known in electronics as the Johnson-Nyquist relation [27, 28]. In analogy with the connection between the compressibility of a system and the small wave-vector limit of the structure factor, we can also show that the capacitance is related to the charge-charge structure factor inside the electrode [26]:

$$\lim_{k\to 0} S_{qq}(k) = \frac{\mathrm{C_{diff}}k_\mathrm{B}T}{M\left\langle\delta q^2\right\rangle} \ , \tag{7}$$

with $\left\langle\delta q^2\right\rangle = \left\langle q^2\right\rangle - \langle q\rangle^2$ the variance of the distribution of the charge per atom. This result holds for both electrodes (with the same $\mathrm{C_{diff}}$), even though $S_{qq}(k)$ may differ for non-zero wave-vectors as the adsorbed fluid is free to adopt different structures on the two electrodes.

The algorithm we use to simulate a metallic electrode maintained at a constant potential follows from the work of Siepmann and Sprik [4], later adapted by Reed *et al.* to the case of electrochemical cells [13]. The electrode consists of explicit atoms bearing a Gaussian charge distribution $\rho_i(\mathbf{r}) = q_i^*\eta^3\pi^{3/2}\exp\left(-\,|\,\mathbf{r}-\mathbf{r}_i\,|^2\,\eta^2\right)$, where η^{-1} is the width of the distribution and where the atomic charge q_i^* of each atom is determined at each time step of the simulation by minimizing $U_c - \sum_{i\in\pm} q_i\Psi_i^0$, with U_c the Coulomb energy, with respect to all the variable

charges simultaneously. Forces acting on the ions are then computed using the minimizing charges.

The distribution of the total charge Q in the constant-potential ensemble is:

$$P(Q|\Delta\Psi) = \int \mathrm{d}\mathbf{r}^N \; P(\mathbf{r}^N|\Delta\Psi)\delta\left(Q - \sum_{i\in+} q_i\right) \qquad (8)$$

with δ the Dirac distribution. The distributions of the total charge can be sampled directly from simulations at the corresponding potentials. However, this sampling is limited to values of the total charge which are close to the average $\langle Q\rangle$. A more accurate estimate can be obtained by combining the data from the simulations performed for various potential differences using histogram reweighting. Indeed, one can show that

$$-\ln P(Q|0) = -\ln P(Q|\Delta\Psi) + \beta Q\Delta\Psi + \beta\Delta\mathcal{F}\,, \qquad (9)$$

with $\Delta\mathcal{F} = \mathcal{F}(\Delta\Psi) - \mathcal{F}(0)$ the difference in free energy (defined by Eq. 4). Each simulation under an applied potential thus provides an estimate of the charge distribution at any other potential, up to the unknown constants $\mathcal{F}(\Delta\Psi)$, which are determined self-consistently in the weighted histogram analysis method (WHAM) [29–31]. Such an approach is well established in other contexts, such as simulations performed at different temperatures, but has not yet been considered for simulations in the constant-potential ensemble.

We investigate several capacitors illustrated in Figure 1: pure water between platinum electrodes and an organic electrolyte, 1-butyl-3-methylimidazolium hexafluorophosphate (BMI-PF_6), either as a pure ionic liquid or as a 1.5 M solution in acetonitrile (MeCN), between graphite electrodes. Details on the systems and molecular models can be found in the Supplementary Information [26]. These combinations of electrodes and electrolytes offer a large contrast of properties: The former is a dielectric capacitor containing only neutral molecules, while the latter contain ions in the gap and are hence "double-layer" capacitors. In addition, in the former case the water molecules form hydrogen-bonds and have a size comparable to that of the electrode atoms, while in the latter all ions and molecules are large so that the electrode appears rather smooth on their scale. Figure 1 also shows the local charge distribution on one of the electrodes for instantaneous configurations of the solvent-based systems under a potential difference. It is strikingly heterogeneous and strongly correlated with the local structure of the adsorbed fluid.

Figure 2 shows that fluctuations of the total charge on the electrodes for both solvent-based systems are Gaussian to a remarkable degree. These statistics imply the validity of the linear response theory over the range of charges shown in Figure 2. The inset shows that $\langle Q\rangle$ is indeed proportional to the applied potential $\Delta\Psi$ with

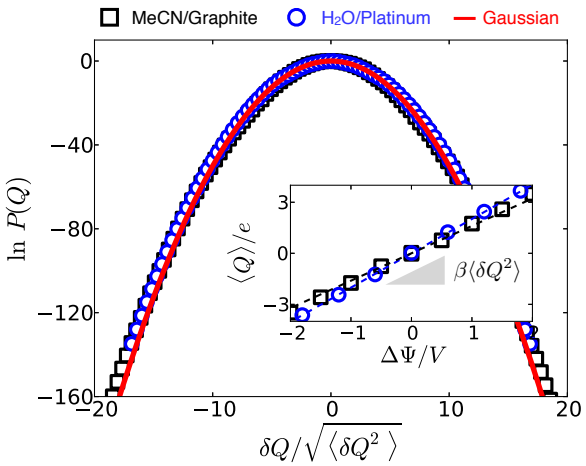

FIG. 2: Probability distribution of the total charge Q. on the electrodes at $\Delta\Psi = 0$ V for the acetonitrile (MeCN) based organic electrolyte between graphite electrodes and for water between platinum electrodes. The data is reported as a function of $\delta Q/\sqrt{\langle\delta Q^2\rangle}$, with $\delta Q = Q - \langle Q\rangle$ and where the variance is 40% larger in the H_2O/Pt case. The red line is a Gaussian distribution with the same mean and variance. In both cases, the distribution is Gaussian. The inset compares the average charge as a function of voltage from simulations (symbols) with lines of slope $\beta\langle\delta Q^2\rangle$: This illustrates the linear response of both systems and the validity of the fluctuation-dissipation relation Eq. (S.4).

a slope $\beta\langle\delta Q^2\rangle$. Such a comparison not only provides information on the physical properties of these two capacitors, but also demonstrates the relevance of this new approach to determine the differential capacitance. The latter is ≈40% larger in the water/Pt case (3.2 vs 2.3 and 2.1 μF.cm^{-2} for the graphite capacitors with the solution in MeCN and pure ionic liquid, respectively). Continuum theory for water between electrodes in the simulated geometry (distance $d = 5.2$ nm between the surfaces), using the permittivity of the SPC/E water model, predicts a capacitance $\epsilon_0\epsilon_r/d = 11.4$ μF.cm^{-2}, indicating that the molecular nature of the interface plays an important role in the overall capacitance (the effective permittivity in the bulk region agrees well with that of SPC/E [17]).

The Gaussian behaviour suggests that the charging process for both systems arises from uncorrelated microscopic events. The local charge induced on the electrode by an interfacial molecule or ion can be analyzed in term of the distribution of individual charges of the electrode atoms. These distributions are reported for both systems as a function of potential in Figure 3. The bimodal distribution in the case of water at Pt arise from the two possible orientations of OH bonds with respect to the surface, which are asymmetric between the positive and negative electrodes and evolves with the potential, as the macroscopic electric field favors or hinders the formation of a hydrogen bond with the surface [17]. For the organic electrolyte on graphite the behaviour is not bimodal, but

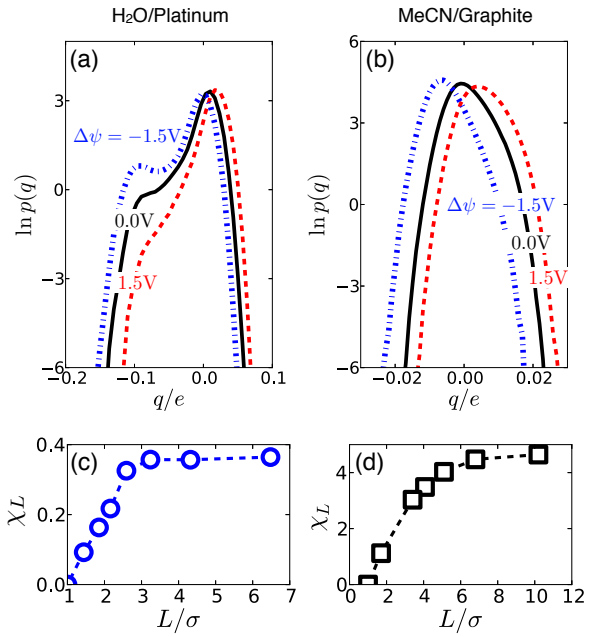

FIG. 3: Distribution of the charge, q_i, on electrode atoms for the H_2O/platinum (a) and MeCN-based organic electrolyte/graphite (b) capacitors, inside the electrodes in the absence and presence of voltage ($\Delta\Psi = \pm 1.5$ V refer to the positive and negative electrodes for 1.5 V). (c) and (d) Variation of the charge fluctuations, χ_L, with increasing electrode area in units of the electrode atom diameter σ (see text).

the distributions are not Gaussian either, where the non-Gaussianity stems from the shape- and size asymmetry of the ions as well as from the dipolar charge distribution of the acetonitrile molecule. As expected, the larger local charges are induced by nearby ions rather than solvent molecules. As the potential changes, the main change in the distribution is a shift of its mean, rather than its shape, as a result of the gradual change in local composition of the interfacial fluid.

The crossover from the non-Gaussian behaviour of the local charge to the Gaussian distribution of Q suggests the existence of a correlation length for the charge distribution inside the electrode, which can be determined by analyzing

$$\chi_L = \frac{\langle \delta Q^2 \rangle_L}{\langle \delta q^2 \rangle} \frac{\sigma^2}{L^2} - 1 \,, \qquad (10)$$

where $\langle \cdot \rangle_L$ is an average over a piece of the electrode $L \times L$ in area, the equivalent electrode atom diameter $\sigma = \sqrt{A/M}$ with A the electrode area and M the corresponding number of atoms, and where as above $\langle \delta q^2 \rangle$ and $\langle \delta Q^2 \rangle$ are the one-body and total charge fluctuations, respectively. For large enough observation area, the distribution is Gaussian with a variance proportional to the area, as expected from the extensivity of the capacitance. The correlation lengths amount to 2-3 water molecules on Pt, consistent with the surface hydrogen bond network (see Figure 1) [1, 17], and ≈ 6 carbon atoms, which correspond to the ionic size, respectively.

The distribution of the total charge is not always Gaussian. Figure 4 compares the distributions at $\Delta\Psi = 0.5$ and 1 V for graphite capacitors with the MeCN-based electrolyte and the pure ionic liquid. While in the former case the distribution is Gaussian with the same variance for both voltages, with the pure ionic liquid this variance increases by a factor of about 2.3 between 0.5 and 1 V. These large fluctuations are reflective of correlations between ions that are not present at low concentration. While the nature of these correlations is beyond of the scope of this work, we note that correlations exist that span the electrode sizes we consider here and cause the fluctuations of the total charge on the electrode to be more or less probable than if it was determined from the sum of many uncorrelated charge centers. These aspects of the pure ionic liquid will be considered in detail elsewhere [33].

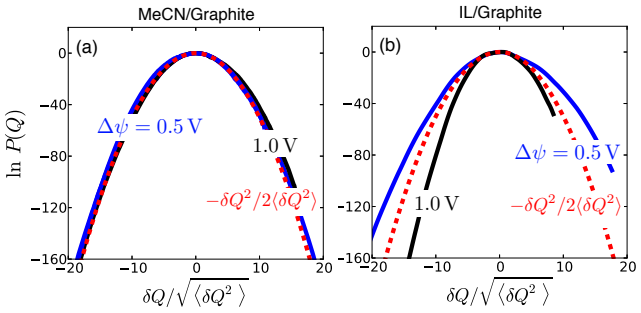

FIG. 4: Distribution of the total charge for the graphite capacitors, with the MeCN-based electrolyte (a) and pure ionic liquid (b). The results for two applied potentials are compared with Gaussian distributions with the same variance. Note that the variance is the same for both potentials in (a) but is larger at 1 V than at 0.5 V in (b).

Combining simulation in the constant-potential ensemble with histogram reweighting techniques has allowed to investigate correlations in the adsorbed fluid and their influence on the electronic properties of the interface. It further provides a unique way to determine the differential capacitance, more accurately than previously, and from a simulation at a *single* value of $\Delta\Psi$. This might prove useful for the study of complex systems such as nanoporous carbon electrodes where the charging mechanism differs from the planar graphite case investigated here [6]. The generalization of this relation to the frequency-dependent capacitance is already exploited experimentally to analyze the electrochemical noise. Molecular simulations combined with importance sampling should allow the investigation of this dynamical aspect [34], not only for the capacitance, but also *e.g.* to explain the voltage-dependence of lubricating properties of IL films on metals [35].

[1] P. Simon and Y. Gogotsi, Nat. Mater. **7**, 845 (2008).
[2] D. Brogioli, Physical Review Letters **103** (2009).
[3] D. Brogioli, R. Zhao, and P. M. Biesheuvel, Energy & Environmental Science **4**, 772 (2011).
[4] N. Boon and R. van Roij, Molecular Physics **109**, 1229 (2011).
[5] U. Bertocci and F. Huet, Corrosion **51**, 131 (1995).
[6] R. A. Cottis, Corrosion **57**, 265 (2001).
[7] M. A. G. Zevenbergen, P. S. Singh, E. D. Goluch, B. L. Wolfrum, and S. G. Lemay, Nano Letters **11**, 2881 (2011).
[8] K. Mathwig, D. Mampallil, S. Kang, and S. G. Lemay, Physical Review Letters **109**, 118302 (2012).
[9] R. Parsons, Chem. Rev. **90**, 813 (1990).
[10] A. A. Kornyshev, J. Phys. Chem. B **111**, 5545 (2007).
[11] Y. Lauw, M. Horne, T. Rodopoulos, and F. Leermakers, Phys. Rev. Lett. **103** (2009).
[12] M. Z. Bazant, B. D. Storey, and A. A. Kornyshev, Phys. Rev. Lett. **106**, 046102 (2011).
[13] B. Skinner, T. Chen, M. S. Loth, and B. I. Shklovskii, Physical Review E **83**, 056102 (2011).
[14] C. Gabrielli, F. Huet, and M. Keddam, The Journal of Chemical Physics **99**, 7232 (1993).
[15] C. Gabrielli, F. Huet, and M. Keddam, The Journal of Chemical Physics **99**, 7240 (1993).
[13] S. K. Reed, O. J. Lanning, and P. A. Madden, J. Chem. Phys. **126**, 084704 (2007).
[17] A. P. Willard, S. K. Reed, P. A. Madden, and D. Chandler, Faraday Discuss. **141**, 423 (2009).
[18] J. Vatamanu, O. Borodin, and G. D. Smith, J. Am. Chem. Soc. **132**, 14825 (2010).
[19] S. Tazi, M. Salanne, C. Simon, P. Turq, M. Pounds, and P. A. Madden, J. Phys. Chem. B **114**, 8453 (2010).
[5] C. Merlet, M. Salanne, B. Rotenberg, and P. A. Madden, J. Phys. Chem. C **115**, 16613 (2011).
[6] C. Merlet, B. Rotenberg, P. A. Madden, P.-L. Taberna, P. Simon, Y. Gogotsi, and M. Salanne, Nature Mater. **11**, 306 (2012).
[22] C. Merlet, C. Péan, B. Rotenberg, P. Madden, P. Simon, and M. Salanne, J. Phys. Chem. Lett. **4**, 264 (2013).
[23] S. Kondrat and A. Kornyshev, J. Phys.: Condens. Matter **23**, 022201 (2011).
[4] J. Siepmann and M. Sprik, J. Chem. Phys. **102**, 511 (1995).
[25] N. Bonnet, T. Morishita, O. Sugino, and M. Otani, Phys. Rev. Lett. **109** (2012).
[26] See Supplementary Material.
[27] J. Johnson, Phys. Rev. **32**, 97 (1928).
[28] H. Nyquist, Phys. Rev. **32**, 110 (1928).
[29] A. M. Ferrenberg and R. H. Swendsen, Phys. Rev. Lett. **63**, 1195 (1989).
[30] S. Kumar, J. M. Rosenberg, D. Bouzida, R. H. Swendsen, and P. A. Kollman, Journal of Computational Chemistry **13**, 1011 (1992).
[31] B. Roux, Computer Physics Communications **91**, 275 (1995).
[1] D. T. Limmer, A. P. Willard, P. Madden, and D. Chandler, Proceedings of the National Academy of Sciences **110**, 4200 (2013).
[33] C. Merlet, M. Salanne, P. Madden, D. Limmer, D. Chandler, R. van Roij, and B. Rotenberg, in preparation.
[34] C. Nieto-Draghi, J. Perez-Pellitero, and J. B. Avalos, Phys. Rev. Lett. **95**, 040603 (2005).
[35] J. Sweeney, F. Hausen, R. Hayes, G. B. Webber, F. Endres, M. W. Rutland, R. Bennewitz, and R. Atkin, Phys. Rev. Lett. **109**, 155502 (2012).

Acknowledgements

BR and DC acknowledge financial support from the France-Berkeley Fund under grant 2012-0007. CM, MS and BR acknowledge financial support from the French Agence Nationale de la Recherche (ANR) under grant ANR-2010-BLAN-0933-02. We are grateful for the computing resources on JADE (CINES, French National HPC) obtained through the project x2012096728. DTL was supported by the Helios Solar Energy Research Center, which is supported by the Director, Office of Science, Office of Basic Energy Sciences of the U.S. Department of Energy under Contract No. DE-AC02-05CH11231.

Supplementary Material

Charge fluctuations in nano-scale capacitors

David T. Limmer, Céline Merlet, Mathieu Salanne, David Chandler,
Paul A. Madden, René van Roij and Benjamin Rotenberg

Simulation details

Dielectric capacitor

Parameters for the water on platinum system are the same as in our previous studies [1, 2]. In this model the water water interactions are described by the SPC/E water model [3] and those between water and the metal atoms are described by the Siepmann and Sprik potential [4]. Both electrodes are modeled as three layers of an FCC crystal with the 111 face in contact with the aqueous solution, consisting of 1008 atoms with nearly 1600 water molecules. The lattice constant is 3.92 Å and the total system size is $3.2 \times 3.3 \times 5.3$ nm^3. The system is periodically replicated in the x and y directions.

Molecular dynamics simulations were conducted in the NVT ensemble using a time step of 2 fs and a Nose-Hoover thermostat with a time constant of 5 ps and a temperature of 298 K. The system is initially equilibrated at constant pressure. Values of the potential used are (0.0,0.195,0.39,0.585, 0.78, 0.975, 1.17, 1.365, 1.56, 1.755, 1.95, 2.145) V. Simulations are equilibrated at each target potential and then run for 5 ns.

Double-layer capacitors

Molecular dynamics simulations are conducted on two different electrolytes surrounded by model graphite electrodes: pure BMI-PF_6 and its corresponding 1.5 M solutions with acetonitrile (MeCN) as a solvent. All molecules are represented by a coarse-grained model in which the forces are calculated as the sum of site-site Lennard-Jones potential and coulombic interactions. Parameters for the ions and carbon atoms are the same as in our previous works [5–8]. In this model, developed by Roy and Maroncelli [9], three sites are used to describe the MeCN and the cation, while the anions are treated as spheres. The model for MeCN was developed by Edwards *et al.* [10]. The parameters are summarized in Supplementary Table I. Each electrode is modelled as three fixed graphene layers, with a distance between carbon atoms within each layer of 1.43 Å and a distance between layers of 3.38 Å. The electrolyte is enclosed between two planar electrodes and two-dimensional periodic boundary conditions are applied, *i.e.* there is no periodicity in the direction perpendicular to the electrodes.

Site	C1	C2	C3	PF_6^-	N	C	Me
q (e)	0.4374	0.1578	0.1848	-0.78	-0.398	0.129	0.269
M ($g.mol^{-1}$)	67.07	15.04	57.12	144.96	14.01	12.01	15.04
σ_i (Å)	4.38	3.41	5.04	5.06	3.30	3.40	3.60
ε_i ($kJ.mol^{-1}$)	2.56	0.36	1.83	4.71	0.42	0.42	1.59

Supplementary Table I: Force-field parameters for the molecules of the electrolytes [5, 9, 10] (geometries of the molecules are available in the aforementioned publications). C1, C2 and C3 are the three sites of the $BMIM^+$ cation, while Me is the methyl group of acetonitrile. Site-site interaction energies are given by the sum of a Lennard-Jones potential and coulombic interactions $u_{ij}(r_{ij}) = 4\varepsilon_{ij}[(\frac{\sigma_{ij}}{r_{ij}})^{12} - (\frac{\sigma_{ij}}{r_{ij}})^{6}] + \frac{q_i q_j}{4\pi\varepsilon_0 r_{ij}}$ where r_{ij} is the distance between sites, ε_0 is the permittivity of free space and crossed parameters are calculated by Lorentz-Berthelot mixing rules. The parameters for the carbon atoms of the graphite electrodes are $\sigma_C = 3.37$ Å and $\varepsilon_C = 0.23$ $kJ.mol^{-1}$ [11].

Molecular dynamics simulations were conducted in the NVT ensemble using a time step of 2 fs and a Nosé-Hoover thermostat [12] with a time constant of 10 ps. The Ewald summation is done consistently with the two-dimensional periodic boundary conditions [13, 14]. Pure ILs and electrolyte solutions are simulated at 400 K and 298 K, respectively. Table II gathers the lengths and number of molecules for the simulation cells. The algorithm used to maintain the potential constant is described in the main text. Five values of potential differences were considered for the MeCN based electrolyte ($\Delta\Psi$ = 0.0, 0.5, 1.0, 1.5 and 2.0 V). Ten values were simulated for the pure ionic liquid ($\Delta\Psi$ = 0.0, 0.2, 0.5, 0.75, 1.0, 1.25, 1.5, 1.75, 1.85 and 2.0 V) in order to ensure a good overlap between the histograms for Q, as required for the histogram reweighting. For each simulation, a 200 ps equilibration is followed by a 5 ns production run for the pure ionic liquid (1 ns for the MeCN based electrolyte for non-zero voltages) from which configurations are sampled every 0.2 ps.

Electrolyte	Temperature (K)	N_{ions}	N_{MeCN}	L_z (nm)
[BMI][PF_6]	400	320	—	12.32
MeCN-[BMI][PF_6]	298	96	896	12.27

Supplementary Table II: Simulation temperature, number of ion pairs, number of MeCN molecules and lengths of the simulation cell in the direction perpendicular to the graphite electrodes for the two electrolytes. The lengths in the x and y directions are the same for all the cells and are equal to 3.22 nm and 3.44 nm respectively.

Derivation of the fluctuation-dissipation relation

The average charge is related to the derivative of the partition function $\mathcal{Z}(\Delta\Psi)$ defined by Eq. (4) of the main text:

$$\langle Q \rangle = \frac{1}{\mathcal{Z}} \int \mathrm{d}\mathbf{r}^N \; e^{-\beta U(\mathbf{r}^N, \mathbf{q}) + \beta Q \Delta\Psi} Q = k_B T \frac{1}{\mathcal{Z}} \frac{\partial \mathcal{Z}}{\partial \Delta\Psi} \; , \tag{S.1}$$

while the average square charge $\langle Q^2 \rangle$ is related to its second order derivative:

$$\langle Q^2 \rangle = (k_B T)^2 \frac{1}{\mathcal{Z}} \frac{\partial^2 \mathcal{Z}}{\partial \Delta\Psi^2} \; . \tag{S.2}$$

The differential capacitance is defined as

$$\mathrm{C_{diff}} = \frac{\partial \langle Q \rangle}{\partial \Delta\Psi} \; . \tag{S.3}$$

Taking the derivative of Eq. S.1 with respect to $\Delta\Psi$ and using Eq. S.2, one finds after elementary algebra that:

$$\langle Q^2 \rangle - \langle Q \rangle^2 = \mathrm{C_{diff}} \times k_B T \; , \tag{S.4}$$

which is the fluctuation-dissipation relation (6) of the main text.

Charge-charge structure factor inside the electrode

The charge distribution inside the electrodes is quantified by the charge-charge structure factor

$$\langle S_{qq}(\mathbf{k})\rangle = \frac{1}{N\left\langle(\delta q)^2\right\rangle}\left\langle\left|\sum_l \delta q_l\ e^{-i\mathbf{k}\cdot\mathbf{r}_l}\right|^2\right\rangle , \tag{S.5}$$

where the sum runs over electrode atoms l, $\delta q_l = q_l - \langle q\rangle$ with q_l their charge and $\mathbf{r}_l$ their position. The small wave-vector limit of $S_{qq}(\mathbf{k})$ is related to the capacitance of the system. Indeed, consider the variance of the total charge:

$$\begin{aligned}\left\langle Q^2\right\rangle - \langle Q\rangle^2 &= \left\langle\sum_{l,m}(\langle q\rangle + \delta q_l)(\langle q\rangle + \delta q_m)\right\rangle - \left\langle\sum_l(\langle q\rangle + \delta q_l)\right\rangle^2 \\ &= \left\langle\sum_{l,m}\delta q_l\delta q_m\right\rangle ,\end{aligned} \tag{S.6}$$

since $\langle\delta q_{l,m}\rangle = 0$. Noting that this variance is equal to $\mathrm{C_{diff}}k_BT$ and using the definition of the charge structure factor, we obtain:

$$S_{qq}(0) = \frac{\left\langle Q^2\right\rangle - \langle Q\rangle^2}{N\left\langle(\delta q)^2\right\rangle} = \frac{\mathrm{C_{diff}}k_BT}{N\left\langle(\delta q)^2\right\rangle} . \tag{S.7}$$

This result holds for both electrodes (with the same $\mathrm{C_{diff}}$), even though $S_{qq}(\mathbf{k})$ may differ for other wave-vectors if the adsorbed fluids adopt different structures. It is worth noting that this relation is similar to the one between the structure factor in a fluid of density ρ and its compressibility χ_T: $\lim_{k\to 0} S(k) = \rho k_B T\chi_T$.

[1] D. T. Limmer, A. P. Willard, P. Madden, and D. Chandler, Proceedings of the National Academy of Sciences **110**, 4200 (2013).
[2] A. P. Willard, D. T. Limmer, P. A. Madden, and D. Chandler, J. Chem. Phys. **138**, 184702 (2013).
[3] H. J. C. Berendsen, J. R. Grigera, and T. P. Straatsma, J. Phys. Chem. **91**, 6269 (1987).
[4] J. Siepmann and M. Sprik, J. Chem. Phys. **102**, 511 (1995).
[5] C. Merlet, M. Salanne, B. Rotenberg, and P. A. Madden, J. Phys. Chem. C **115**, 16613 (2011).
[6] C. Merlet, B. Rotenberg, P. A. Madden, P.-L. Taberna, P. Simon, Y. Gogotsi, and M. Salanne, Nature Mater. **11**, 306 (2012).
[7] C. Merlet, M. Salanne, and B. Rotenberg, J. Phys. Chem. C **116**, 7687 (2012).
[8] C. Merlet, M. Salanne, B. Rotenberg, and P. Madden, Electrochimica Acta **101**, 262 (2013).
[9] D. Roy and M. Maroncelli, J. Phys. Chem. B **114**, 12629 (2010).
[10] D. M. Edwards, P. A. Madden, and I. R. McDonald, Molecular Physics **51**, 1141 (1984).
[11] M. W. Cole and J. R. Klein, Surface Science **124**, 547 (1983).
[12] G. J. Martyna, M. L. Klein, and M. Tuckerman, J. Chem. Phys. **97**, 2635 (1992).
[13] S. K. Reed, O. J. Lanning, and P. A. Madden, J. Chem. Phys. **126**, 084704 (2007).
[14] T. R. Gingrich and M. Wilson, Chem. Phys. Letters **500**, 178 (2010).